Journal of Electroanalytical Chemistry

Spectroelectrochemical and DFT approaches to the study of croconic acid adsorption at gold electrodes in acidic solutions.

--Manuscript Draft--

Manuscript Number:	JELECHEM-D-21-00416R1
Article Type:	SI:Physical Electrochemistry
Keywords:	croconic acid; croconate anions; gold; thin film electrodes; ATR-SEIRAS; DFT
Corresponding Author:	Antonio Rodes Universidad de Alicante Alicante, Spain
First Author:	Antonio Rodes
Order of Authors:	Antonio Rodes
	William Cheuquepán, Dr
	José Manuel Orts, Prof
Manuscript Region of Origin:	SPAIN
Abstract:	The adsorption of species coming from croconic acid (4,5-dihydroxy-4-cyclopentene-1,2,3-trione, H 2 C 5 O 5 , CA) at gold electrodes was studied spectroelectrochemically in aqueous perchloric acid solutions. Voltammetric experiments suggest the existence of reversible adsorption processes in the potential range between 0.30 and 0.80 V RHE. Surface-Enhanced Infrared Reflection Absorption Spectroscopy experiments under Attenuated Total Reflection conditions show potential-dependent adsorbate bands in the latter potential range that, according to Density Functional Theory calculations, can be assigned to adsorbed croconate. Calculated optimized geometry corresponds to bonding of croconate species to the gold surfaces involving two oxygen atoms in a bidentate configuration, with the molecular plane perpendicular to the metal surface for low and high crocoanate coverage. For intermediate coverage, lateral repulsions between neighbor croconate adsorbates give rise to the tilting of the molecular plane. The broadening and splitting at high electrode potentials of the C-O stretching bands for adsorbed croconate can be explained by invoking the existence of collective vibrational modes appearing at high coverage. The cyclic voltammograms recorded in the CA-containing solutions also show the existence of reversible redox processes at potentials below 0.30 V involving adsorbed species, which are detected in the ATR-SEIRA spectra collected in this potential range.

Spectroelectrochemical and DFT approaches to the study of croconic acid adsorption at gold electrodes in acidic solutions.

William Cheuquepán[c], Antonio Rodes[a,b,*], José Manuel Orts[a,b]

[a] Departamento de Química Física and [b] Instituto Universitario de Electroquímica. Universidad de Alicante. Apartado 99, E-03080 Alicante, Spain

[c]Departamento de Química, Universidad de Burgos, Pza. Misael Bañuelos s/n, E-09001 Burgos, Spain

*Corresponding author

Highlights

- Croconate anions adsorb at Au electrodes in croconic acid-containing solutions.
- Croconate species bons in a bidentate configuration with O atoms on top positions.
- Adsorption occurs with the molecular plane (quasi)normal to the metal surface.
- Adsorption causes significant changes on the geometry and symmetry of croconate.
- Collective vibrations broaden and split croconate bands at high coverage.

Spectroelectrochemical and DFT approaches to the study of croconic acid adsorption at gold electrodes in acidic solutions.

William Cheuquepán[c], Antonio Rodes[a,b,*], José Manuel Orts[a,b]

[a] Departamento de Química Física and [b] Instituto Universitario de Electroquímica. Universidad de Alicante. Apartado 99, E-03080 Alicante, Spain

[c]Departamento de Química, Universidad de Burgos, Pza. Misael Bañuelos s/n, E-09001 Burgos, Spain

*Corresponding author

Table 1. Selected geometry parameters for the optimized structure of discharged croconate on Au(111) (Θ=1/9).

C-O bond length /pm	C-C bond length /pm	O-Au bond length /pm	Au-Au-O angle / º
d C1-O1 =121	d C1-C2 = d C1-C3 =154	d O5-Au = 227	Θ Au-Au-O5 = 93.3
d C2-O2 = d C3-O3 =122	d C2-C4 = d C3-C5 =148	d O4-Au = 229	Θ Au-Au-O4 = 90.5
d C4-O4 = d C5-O5 =127	d C4-C5 =144		

Table 2. Selected geometrical parameters for the optimized structures of croconate anion ($C_5O_5^{2-}$; q=-2), cyclopentanpentone (C_5O_5; q=0) and croconic acid ($H_2C_5O_5$) in gas phase.*

	d C-O / pm	d CC / pm	d O-H / pm
C_5O_5 (Cyclopentanpentone)	122	155	-
$H_2C_5O_5$ (Croconic acid)	dC1-O1 = 121 dC2-O2 = dC3-O3 = 123 dC4-O4 = dC5-O5 = 133	dC1-C2 = dC1-C3 = 153 dC2-C4 = dC3-C5 = 148 dC4-C5 = 138	99
$C_5O_5^{2-}$ (Croconate)	125	150	-

*Numbering of C and O atoms in croconic acid follows that of adsorbed croconate, with O4 and O5 atoms bonded to hydrogen (instead of to the surface gold atoms).

Table 3. Selected calculated harmonic frequencies (in cm^{-1}) and band assignments for discharged croconate on Au(111) surfaces at various coverages.

θ= 1/9	Assignment	θ= 2/9	Assignment	θ= 1/3	Assignment
1754	Str C1-O1	1765 1757	Str C1-O1, ip Str C1-O1, oop	1776 1765, 1764	Str C1-O1, ip Str C1-O1, oop
1723	Sym str C2-O2+ C3-O3	1725 1674	Sym str C2-O2+ C3-O3, ip Sym str C2-O2+ C3-O3, oop	1738 1692, 1691	Sym str C2-O2+ C3-O3, ip Sym str C2-O2+ C3-O3, oop
1657	Asym str C2-O2+ C3-O3	1658 1650	Asym str C2-O2+ C3-O3, ip Asym str C2-O2+ C3-O3, oop	1701 1672, 1668	Asym str C2-O2+ C3-O3, ip Asym str C2-O2+ C3-O3, oop
1498	Sym str O4-C4-C5-O5	1469 1464	Sym str O4-C4-C5-O5, ip Sym str O4-C4-C5-O5, oop	1558 1490,1489	Sym str O4-C4-C5-O5, ip Sym str O4-C4-C5-O5, oop
1401	Asym str O4-C4-C5-O5	1413 1410	Asym str O4-C4-C5-O5, ip Asym str O4-C4-C5-O5, oop	1535 1515, 1515	Asym str O4-C4-C5-O5, ip Asym str O4-C4-C5-O5, oop

- Only the main contribution to the normal mode is given.
- ip : in- phase ; oop= out of phase (these refer to the eventual dephasing of the movements between different molecules contributing to the collective vibrational mode)

Figure(s)

Click here to access/download;Figure(s);CA_jeac_FIG1.tif

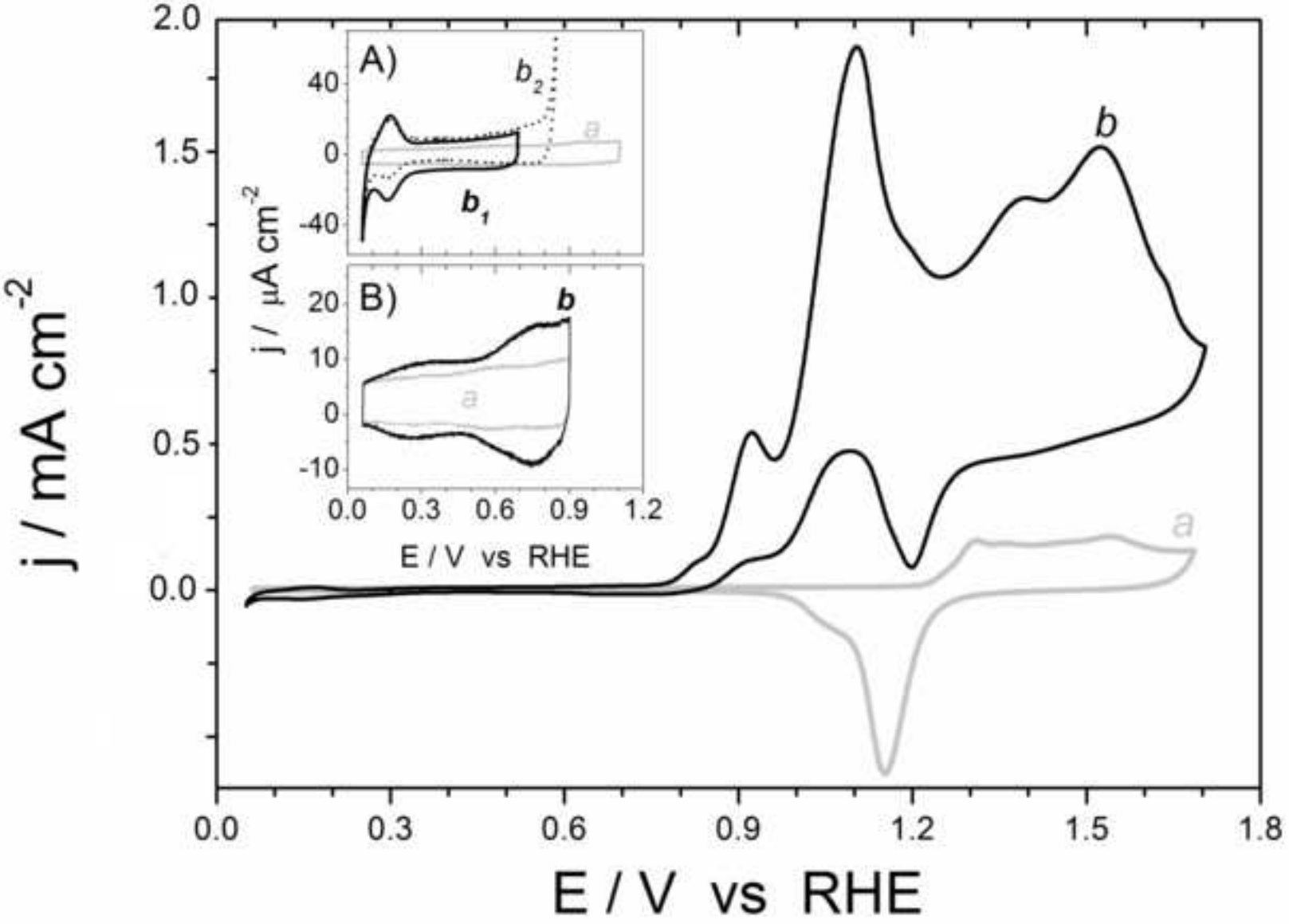

Figure(s)

Click here to access/download;Figure(s);CA_jeac_FIG2.tif

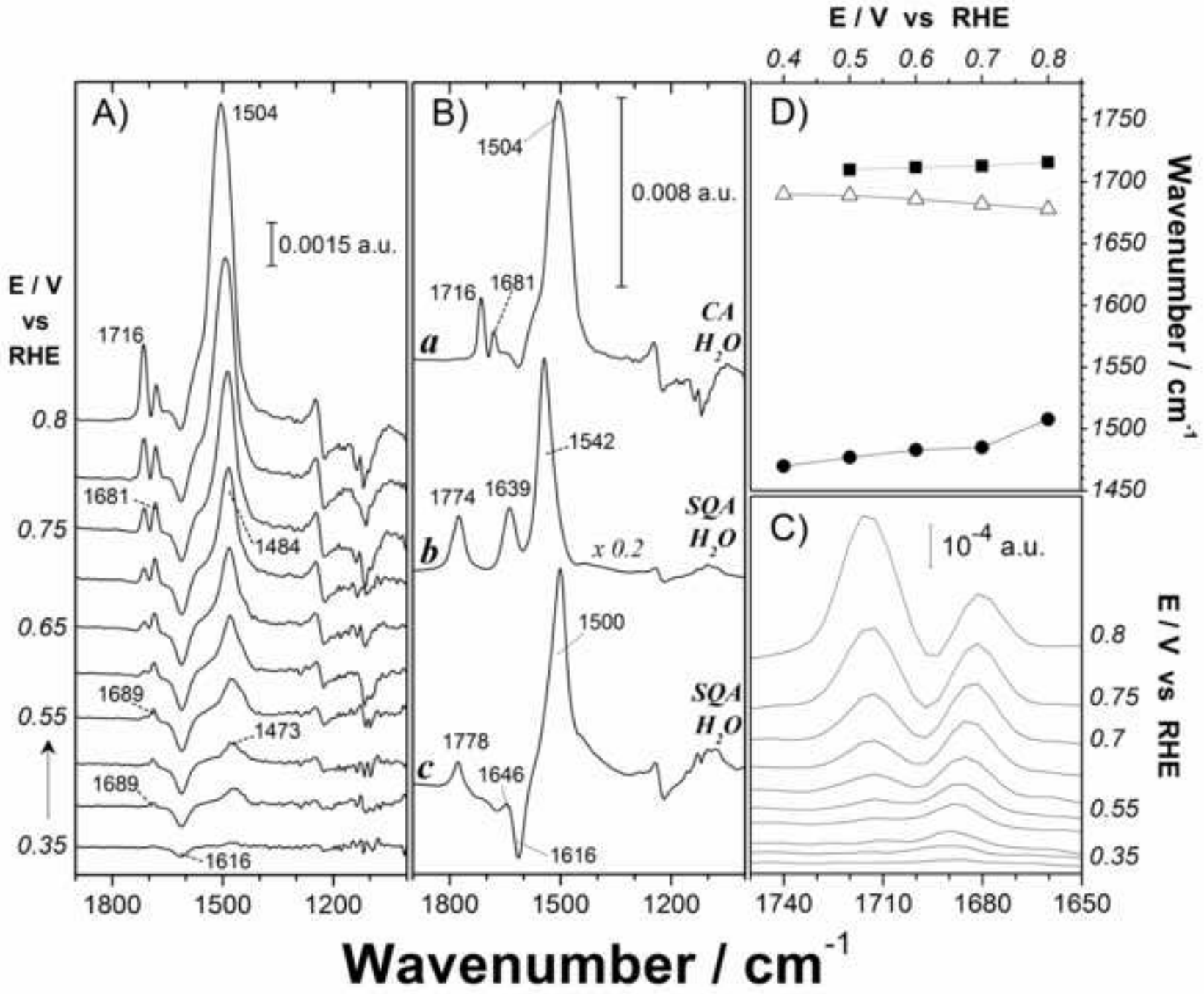

Figure(s)

Click here to access/download;Figure(s);CA_jeac_FIG3.tif

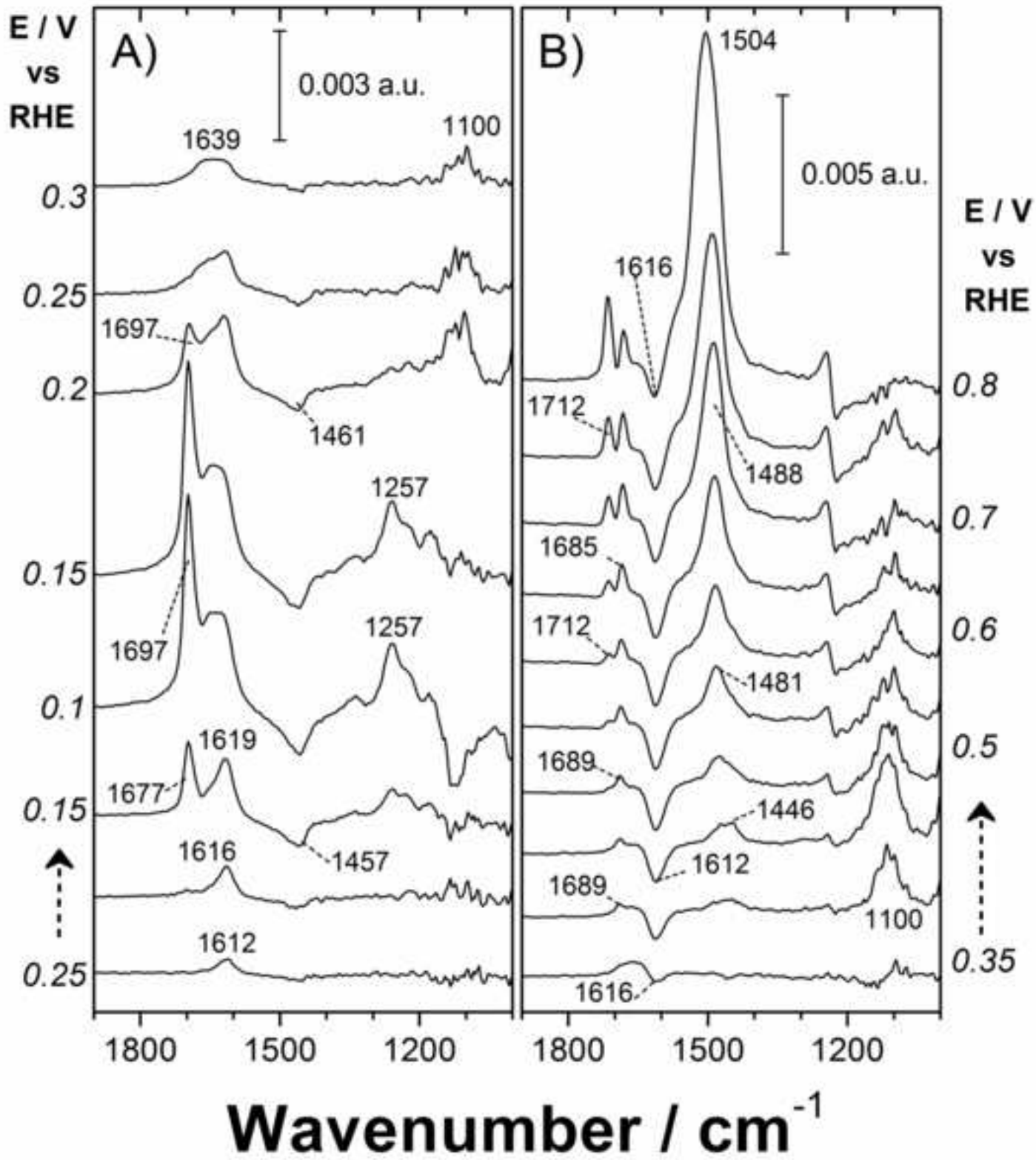

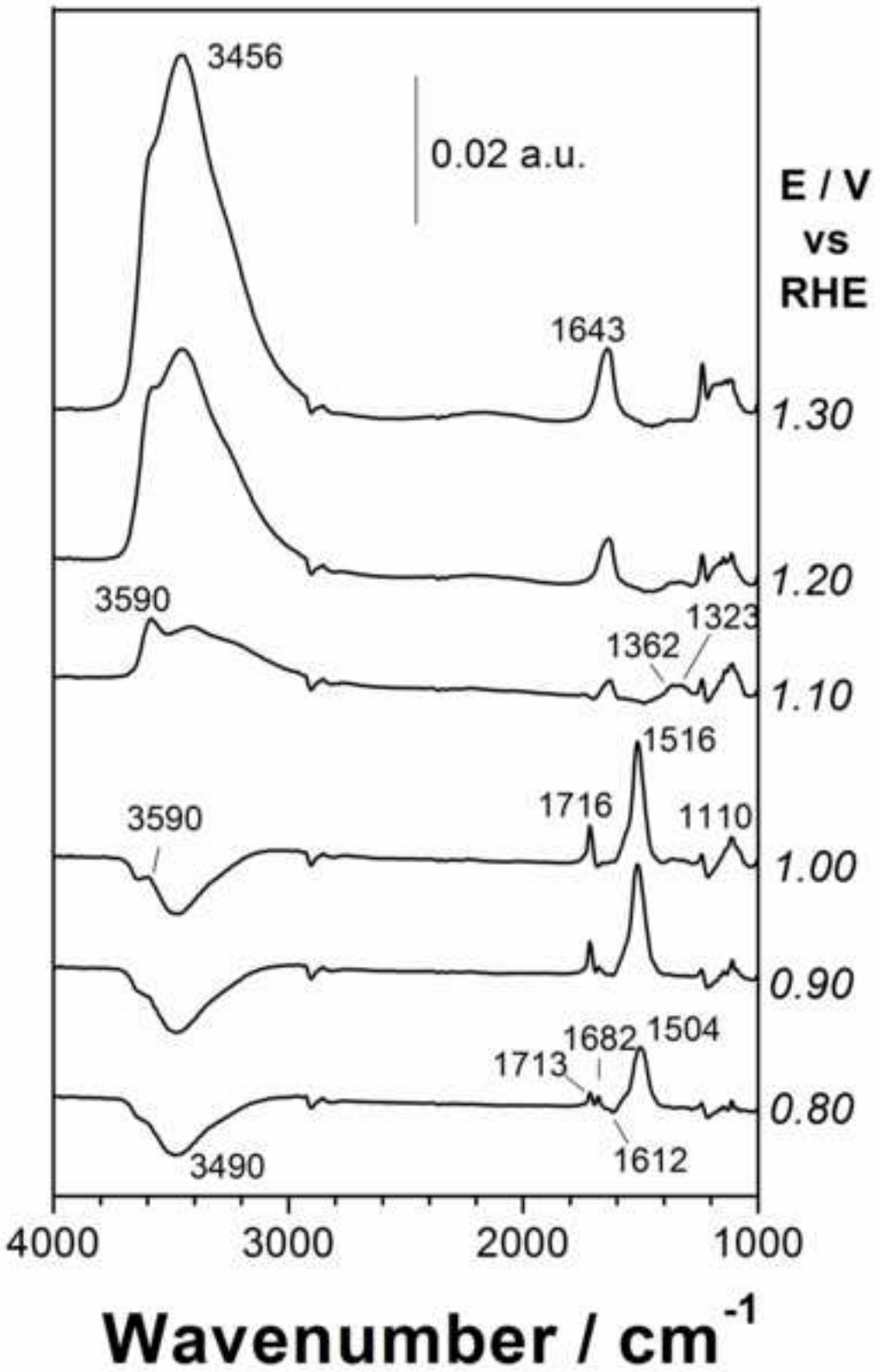

Figure(s)

Click here to access/download;Figure(s);CA_jeac_FIG5.tiff

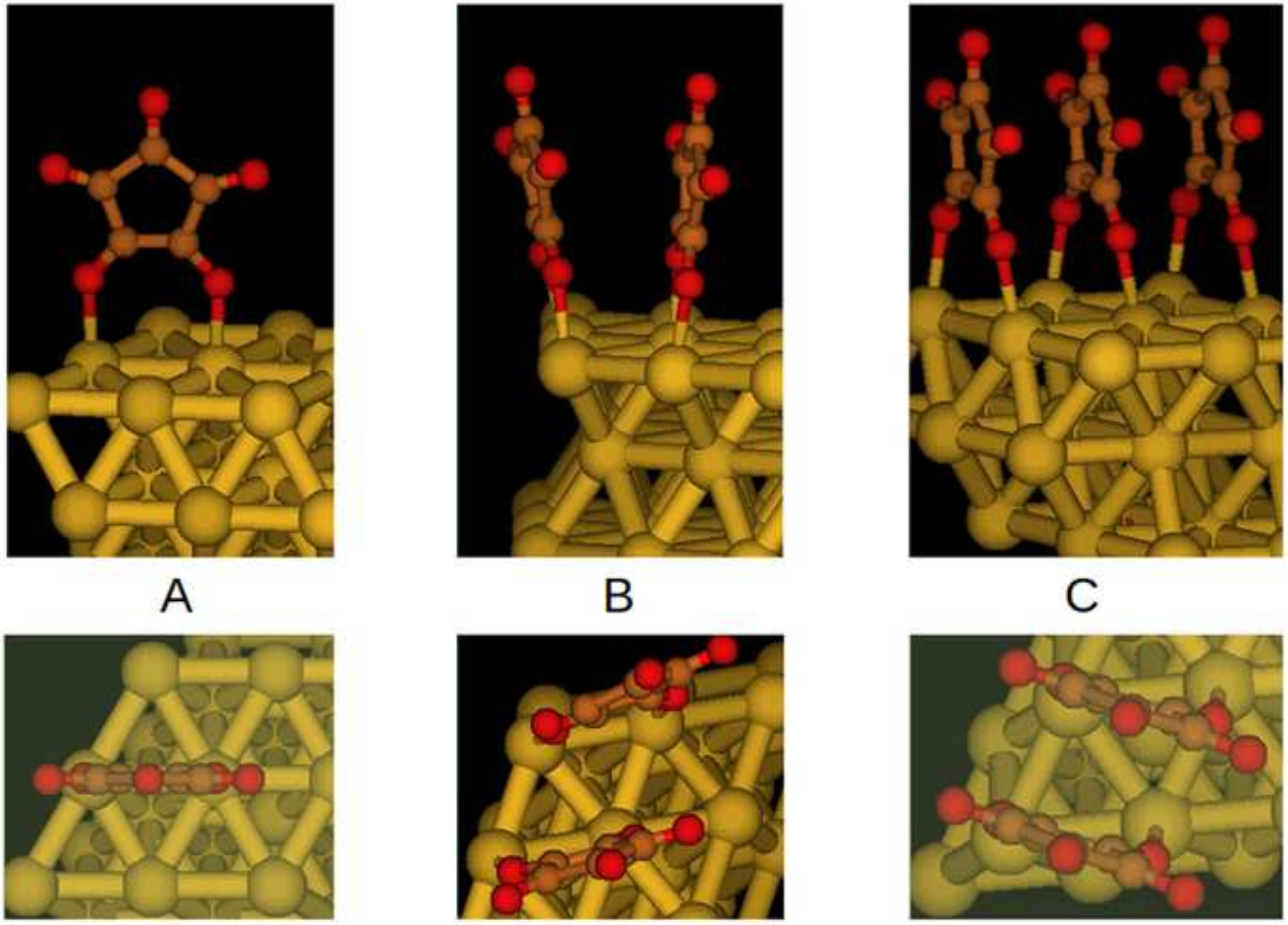

Figure(s) Click here to access/download;Figure(s);CA_jeac_Scheme 1.tiff

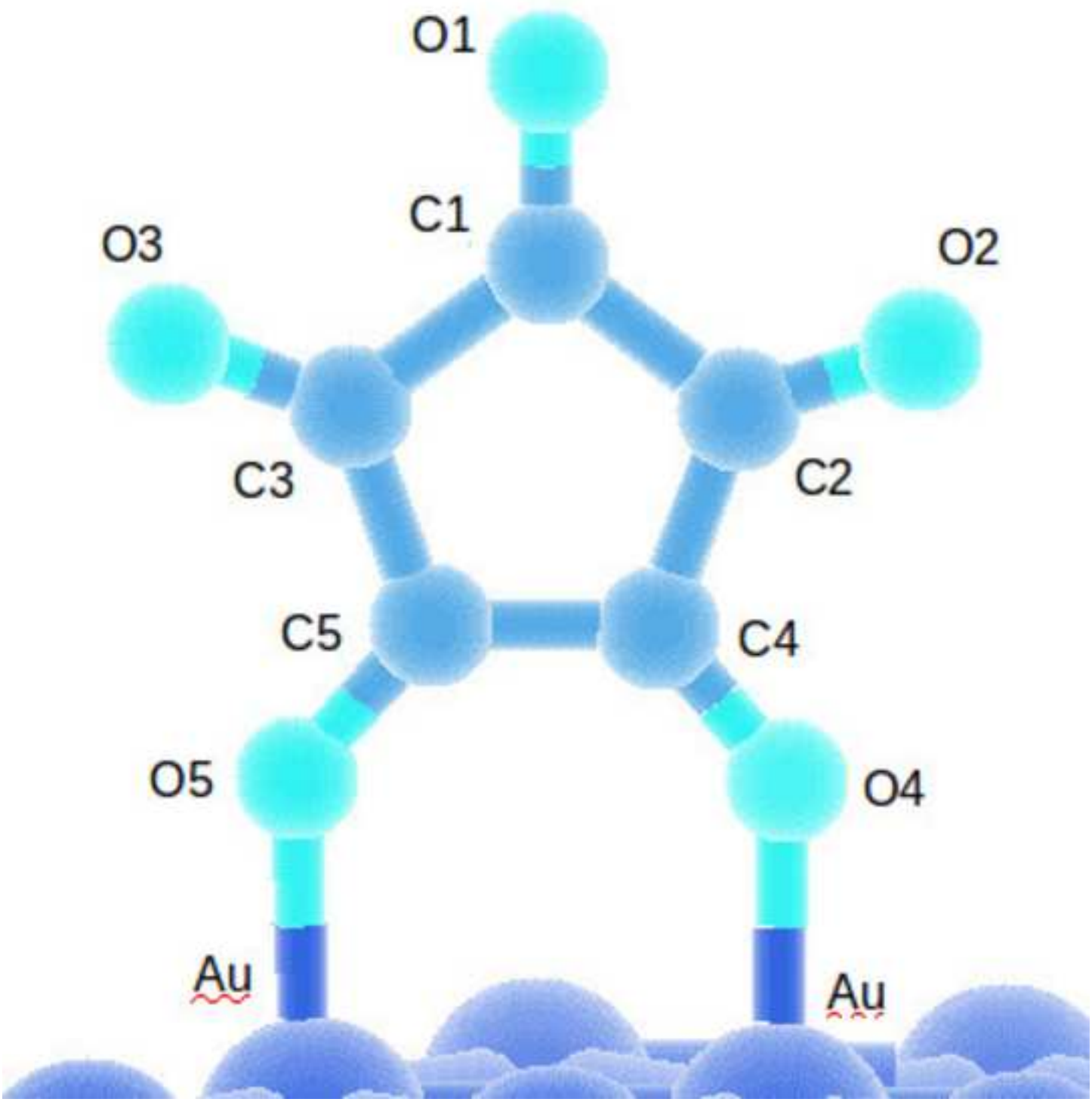

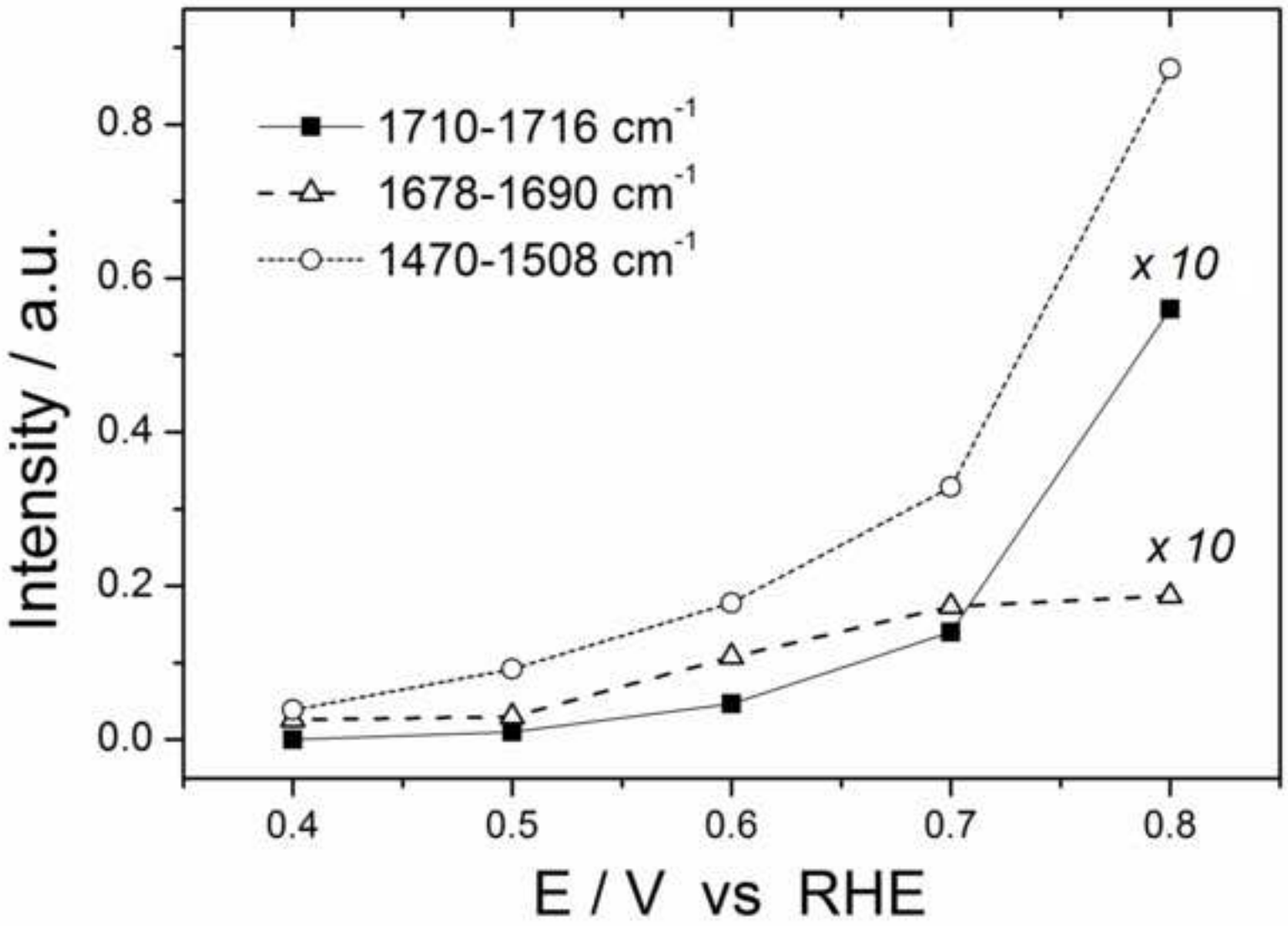

Spectroelectrochemical and DFT approaches to the study of croconic acid adsorption at gold electrodes in acidic solutions.

William Cheuquepán[c], Antonio Rodes[a,b,*], José Manuel Orts[a,b]

[a] Departamento de Química Física and [b] Instituto Universitario de Electroquímica. Universidad de Alicante. Apartado 99, E-03080 Alicante, Spain

[c]Departamento de Química, Universidad de Burgos, Pza. Misael Bañuelos s/n, E-09001 Burgos, Spain

*Corresponding author

Abstract

The adsorption of species coming from croconic acid (4,5-dihydroxy-4-cyclopentene-1,2,3-trione, $H_2C_5O_5$, CA) at gold electrodes was studied spectroelectrochemically in aqueous perchloric acid solutions. Voltammetric experiments suggest the existence of reversible adsorption processes in the potential range between 0.30 and 0.80 V RHE. Surface-Enhanced Infrared Reflection Absorption Spectroscopy experiments under Attenuated Total Reflection conditions show potential-dependent adsorbate bands in the latter potential range that, according to Density Functional Theory calculations, can be assigned to adsorbed croconate. Calculated optimized geometry corresponds to bonding of croconate species to the gold surfaces involving two oxygen atoms in a bidentate configuration, with the molecular plane perpendicular to the metal surface for low and high crocoanate coverage. For intermediate coverage, lateral repulsions between neighbor croconate adsorbates give rise to the tilting of the molecular plane. The broadening and splitting at high electrode potentials of the C-O stretching bands for adsorbed croconate can be explained by invoking the existence of collective vibrational modes appearing at high coverage. The cyclic voltammograms recorded in the CA-containing solutions also show the existence of reversible redox processes at potentials below 0.30 V involving adsorbed species, which are detected in the ATR-SEIRA spectra collected in this potential range.

Keywords: croconic acid; croconate anions; gold; thin film electrodes; ATR-SEIRAS; DFT

1. Introduction

Croconic acid (4,5-dihydroxy-4-cyclopentene-1,2,3-trione, $H_2C_5O_5$, CA) is one of the so-called oxocarbons ($H_2C_nO_n$) [1-3]. As in the case of deltic (n=3), squaric (n=4), and rhodizonic (n=6) acids, croconic acid (n=5) is characterized by its relatively high acidic dissociation constant values ($pK_{a,1}$ and $pK_{a,2}$ equal to 0.80 and 2.24, respectively [4, 5]), which are related to the remarkable stability of the oxocarbon anions coming from electronic π-delocalization [2, 3]. Besides, the existence of strong intermolecular hydrogen bonds determines the structures of croconic acid both in solid crystals [6] and when forming homogeneous [7] or heterogeneous 2D self-assembled phases[8, 9]. In the case of croconate salts, stacking of flat anion units has been reported [10, 11].

In recent years, croconic acid and its derivatives have been the object of a significant number of studies exploring a variety of their properties. In this way, CA crystals show a strong ferroelectric behavior [12, 13], also observed in the case of croconic acid thin films [14, 15]. Density Functional Theory (DFT) has been employed to calculate mechanical, thermodynamic and optical properties of solid croconic acid [16-18]. In this latter respect, the experimental SERS spectra of croconic acid and croconate anions adsorbed at silver surfaces have been reported [19]. It is worth mentioning also the publication of DFT calculations of the infrared and Raman spectra for croconate anions both in the gas phase and in solution [20]. From an applied point of view, the use of croconic acid disodium salt as a Li-ion battery electrode has been proposed [21]. Kikuchi et al studied the growth behavior of anodic porous alumina in CA solutions [22]. CA has also been employed both as reducing and capping agent for the synthesis of gold nanoparticles [23]. Finally, it is remarkable the strong visible or near-IR absorption of croconic acid derivative dyes with applications in optoelectronics or biomedicine [24, 25].

Some papers have been published on the electrochemical reactivity of croconic acid and some of its derivatives both in non-aqueous solvents [26-30] and in aqueous solutions [31-43]. Fleury et al reported the reduction of CA at mercury electrodes in aqueous solutions [31-33] and proposed the formation of various reduction products. In this way, the formation of stable products corresponding to a transfer of either two (RH_2) or four (RH_4) electrons per CA (R) molecule were detected (probably related to the reduction of one or two of the carbonyl groups in CA to –CHOH- moieties) [32]. A one-electron process (involving a dimerization step to form a pinacol-like species, RH-RH) has also been reported [32]. Sazou and Kokkinidis [34] and Fabre et al. [28] studied the electrochemical oxidation of CA in aqueous solutions on platinum and glassy carbon electrodes (GCE), respectively. In these two papers the formation of leuconic acid (ciclopentanepentone) was proposed to take place in a direct two-electron oxidation process.

This is in contrast with results in non-aqueous solvents showing the existence of two monoelectronic steps in different potential range due to the stability of the intermediate anion radical species [26-30, 44]. The hydration of leuconic acid has been invoked to explain the irreversibility of the CA oxidation reaction in aqueous media [34]. Larm et al studied also the electrochemical behavior of croconic acid at GCE and platinum electrodes and reported the existence of reduction processes, not observed with squaric acid [23], undergone by the species formed upon CA oxidation.

In the previously mentioned works, no clear evidence was provided on the presence and nature of adsorbed species formed at electrodes in contact with oxocarbon-containing solutions. It was later proven that the electrochemical reactivity of oxocarbons at platinum electrodes is characterized by the existence of parallel reaction paths involving dissociation steps that lead to the formation of adsorbed carbon monoxide [35-42]. This adsorbate was identified from the corresponding in situ infrared spectra in the case of squaric [36, 40, 42], croconic [38] and rhodizonic [39]acids. In the case of squaric acid, the formation of other adsorbates different from CO (namely, adsorbed squarate anions) has also been detected spectroscopically [40, 42]. The adsorption of the squarate anions was also detected in the case of gold electrodes, for which the formation of adsorbed carbon monoxide upon dissociation of squaric acid is not observed [42, 43]. DFT calculations [42, 43] confirmed that adsorbed squarate anions are bonded to the gold surfaces in a bidentate configuration through two oxygen atoms, with the molecular plane perpendicular to the metal surface, this configuration allowing for its experimental spectroscopic detection. Besides, it has been proven that some spectroscopic features (namely, band splitting and broadening) observed at high adsorbate coverage (obtained at high solution concentrations and/or electrode potentials) could be ascribed to collective vibrational modes of the adsorbed squarate (sub)monolayer [43].

In this work we present new spectroelectrochemical results regarding the electrode processes taking place at gold thin film electrodes in aqueous acidic solutions containing croconic acid. Potential-dependent ATR-SEIRAS (Surface Enhanced Infrared Reflection Absorption Spectroscopy under Attenuated Total Reflection conditions) spectra were collected in a wide potential range where several reduction and oxidation processes are voltammetrically detected. In this preliminary work, special attention is given to the spectroscopic characterization of the adsorbed layers formed in the double-layer region. As a guide for the interpretation of the experimental spectra, a DFT study is carried out to obtain optimized geometries and vibrational frequencies for croconate adsorbed at model Au(111) surfaces. This choice is determined by the preferential (111) orientation of the gold thin film electrodes used in the ATR-SEIRAS

experiments [45-47]. Regarding the utility of the DFT approach for the calculation vibrational behavior of adsorbed species, it has to be recalled here that changes in intramolecular bonding in adsorbates with respect to the corresponding free species would make unclear an analysis based on calculated or experimental values for the same (or related species) in gas phase or in solution [48]. This holds specially in the case of croconate species due to the drastic changes in the molecular symmetry upon adsorption. The present study is connected to previous works published by our group on the adsorption behavior of related oxocarbons (namely, squaric acid) on gold electrodes [42, 43]. Special attention is given to the effect of croconate coverage on the infrared spectra for this species, which shows typical broadening and splitting effects already described for other adsorbed species [43, 49, 50].

2. **Experimental**

Working solutions were prepared from solid croconic acid disodium salt (97% Alfa Aesar), concentrated perchloric acid (Merck Suprapur®) and ultrapure water (18.2 MΩ·cm, TOC 50 ppb max, Elga Vivendi). These solutions were deaerated with Ar (N50, Air Liquide) and kept under an atmosphere of this gas during the experiments.

The voltammetric measurements were performed with a eDAQ EA 161 potentiostat, a EG&G 175 signal generator and a eDAQ e-corder ED401 recording system. All the voltammetric and in situ infrared experiments were performed in a glass spectroelectrochemical cell with a reversible hydrogen electrode (RHE) and a gold wire as the reference and counter electrodes, respectively. Gold thin films used as working electrode in the voltammetric and internal reflection infrared spectroscopy experiments were deposited on one of the faces of a low oxygen-content silicon prism beveled at 60^{o} (Pastec Ltd, Japan). The deposition of a 20 nm-thick gold thin film (99.999%, Kurt J. Lesker Ltd.) was carried out by thermal evaporation in the vacuum chamber of a PVD75 (Kurt J. Lesker Ltd.) coating system at a base pressure around 10^{-6}Torr. The thickness of the gold film and the deposition rate (fixed at 0.006 nm·s^{-1}) were controlled with a quartz crystal microbalance. Once in the spectroelectrochemical cell, the gold thin film electrodes were cleaned by applying a few voltammetric cycles up to 1.70 V RHE in the 0.1 M $HClO_4$ solution.

In situ infrared experiments were carried out either with a Nexus 8700 or with a IS50R (ThermoScientific) spectrometers, both equipped with MCT-A detectors and a wire grid ZnSe polarizer. The spectroelectrochemical cell [51, 52] was placed at the top of a Veemax (Pike Tech.)

reflectance accessory. All the spectra were collected with p-polarised radiation with a resolution of 8 cm^{-1}. The spectra are plotted in absorbance units (a.u.) as $-\log(R/R_o)$, where R and R_o represent the single beam sample and reference reflectivity spectra, respectively. Thus, positive/negative bands correspond, respectively, to gain/loss of species in the sample spectrum with respect to the reference spectrum collected at 0.30 V in the CA-containing solution. In some experiments, each sample spectrum was obtained after stepping the electrode to a potential value which is kept constant during the collection of 100 interferograms. In other experiments, the spectra were collected in a rapid scan mode while the electrode potential was swept at 2 $mV \cdot s^{-1}$ in the potential range indicated for each experiment. Each spectrum was the average of a set of 104 interferograms which were collected in ten seconds, thus corresponding to a 20 mV interval centered at the indicated potential value.

3. Computational details

Density Functional Theory calculations have been used in the generalized gradient approximation (GGA) using the functional proposed by Perdew, Burke and Ernzehof [53, 54], in order to obtain microscopic information about the adsorption of croconate species on model Au surfaces with (111) orientation. In particular, we obtained optimized adsorption geometries as well as theoretical vibrational frequencies (within the harmonic approximation).

All the calculations reported in this paper were carried out with the Vienna Ab-Initio Simulation program [55-58], using the Projector-Augmented Wave (PAW) method [59]. The cutoff energy for the plane wave basis was set to 400 eV.

The models used for studying the adsorption of croconate (from one to three molecular units, depending on the coverage under study) on the model Au(111) surfaces were slabs of four atomic layers (with 9 gold atoms each, arranged in a (3x3) 2D structure). The optimized geometries of the croconate adsorbates were obtained by allowing the full relaxation of the atomic coordinates of the carbon and oxygen atoms, while maintaining frozen those of the metal centers. For obtaining the optimized geometry at low coverage, several initial adsorbate geometries were tested, that differ in the orientation of the molecular plane with respect to the surface, and the position of the oxygen atoms close to the surface, relative to the surface metal atoms. For the medium and high coverages, the initial geometry of each adsorbate species was the optimized geometry obtained in the low coverage range. In all calculations the gold atoms were kept fixed at their bulk positions, with a nearest-neighbor metal-metal distance of 0.29520

nm, obtained by fitting to a Murnaghan equation of state. A vacuum region of more than 12 Angstrom allowed for the decoupling of the interactions between the surfaces of periodic slab replicas.

The Methfessel-Paxton method [60] (second order, σ=0.2 eV) was chosen for smearing, and the automated Monkhorst-Pack method [61] sampled the reciprocal space using a gamma-centered (5 x 5 x 1) k-points scheme. The convergence criteria for the electronic and geometric convergences were respectively: energy changes below 10^{-5} eV, and Hellman-Feynman forces on all atoms below 0.02 eV/Angstrom.

For the optimization in gas phase of the croconate, cyclopentanpentone and croconic acid species, a cubic simulation box with a length of 16 Angstrom was used, and the Brillouin zone sampling was restricted to only the gamma k-point. These calculations used the same cut-off and convergence criteria that in the case of the adsorbed species. In the case of the gas phase species, additional optimizations were carried out with the following convergence criteria: energy changes below 10^{-6} eV, and Hellman-Feynman forces on all atoms below 0.005 eV/Angstrom. The resulting geometries and harmonic frequencies were essentially identical to those obtained with milder convergence criteria.

The calculated vibrational frequencies for adsorbates (given as obtained, without any frequency scaling) were obtained using the harmonic approximation with atomic displacements of +/- 0.015 Angstrom in each spatial coordinate. Estimated relative errors (from previous combined theoretical-experimental studies) are in average below 2-3% of the theoretical frequency value. Both the optimized geometries and the vibrational movements of the different normal modes were visualized using Jmol [62].

4. Experimental results

Figure 1 shows cyclic voltamograms (CV) obtained in aqueous perchloric acid solutions for an evaporated gold thin film electrode. The CVs in the double layer region can be observed in both A and B insets (curves a). Curve a in the main box corresponds to the voltammetric curve recorded in the potential range between 0.10 and 1.70 V, showing apparently the characteristic profile for the oxidation/reduction of a polyoriented gold surface in the perchloric acid solution. However, and as previously reported for sputtered samples [47], thin gold films slowly grown on silicon substrates predominantly consist of sites belonging to (111) terraces (as witnessed

from the intensity of the oxidation peak at ca. 1.53 V). On the other hand, the peak at ca. 1.30 V indicates the presence of adsorption sites with other orientations.

In the presence of 10 mM CA, the corresponding cyclic voltammograms show a complex oxidation profile for potentials above 0.80 V (curve b). Several oxidation peaks can be observed between 0.90 and 1.70 V that overlap with the currents due to the oxidation of the gold surface. In the negative-going sweep, the CA oxidation tail between 1.70 and 0.90 V overlaps with the gold oxide reduction peak appearing around 1.20 V.

In the double layer region, the cyclic voltammogram recorded with the gold thin film electrode in the presence of CA shows an excess of voltammetric charge with respect to the CA-free solution (curves b1 and a, respectively, in inset A). The excess current in the CA-containing solution is rather featureless when compared to that observed in the case of SQA, which shows two broad features at ca. 0.30 and 0.75 V (curve b in inset B)that are related to adsorption-desorption processes as witnessed by in-situ infrared spectra (see references [42, 43]and below). Another difference between the cyclic voltammograms for CA- and SQA-containing solutions is related to the observation in the former case of a redox peak centered at ca. 0.15 V. Extending the positive-going sweep up to 0.85 V (thus, entering into the potential range where the CA electroxidation already proceeds (curve b2 in inset A)) causes a decrease of the intensity of the reduction peak at 0.15 V. This suggests that some species, involved in the redox processes below 0.30 V, could be oxidatively removed from the vicinity of the electrode surface at potentials between 0.80 and 0.85V. However, curve b1 is restored in the subsequent voltammetric cycles between 0.1 and 0.70 V.

ATR-SEIRAS experiments have been carried out with the gold thin film electrodes in a 10 mM CA + 0.1 M $HClO_4$ solution in order to shed some light on the nature of the adsorbed species giving rise to the voltammetric features presented above. The high surface sensitivity and specificity of these spectra (both related to the enhanced infrared absorption from adsorbates associated to the SEIRA effect) [63, 64] may help for this purpose. In this way, the bands appearing in the potential-dependent spectra are due to adsorbed species being formed/consumed at the electrode surface without strong interferences from dissolved species and bulk water molecules.

Panel A in Figure 2 shows a set of spectra collected while the electrode potential was swept between 0.30 and 0.80 V (see experimental section for details). These spectra show positive bands in the region between 1750 and 1400 cm^{-1} that can be related to the adsorption of species coming from CA. At 0.45 V the spectrum shows a single band at ca. 1473 cm^{-1} together with a small feature at 1689 cm^{-1}. At potentials above 0.50 V, a new feature appears in the spectra at

ca. 1712 cm^{-1} whereas the frequency of the main peak is shifted to 1504 cm^{-1} at 0.80 V. The intensities of all these features become higher as the electrode potential is increased up to 0.80 V. At the same time, it can be noticed in Figure 2A that the main feature in the spectra broadens and becomes asymmetric for more positive potentials, with shoulders appearing at higher wavenumbers. No additional features related to species coming from CA seem to appear in the spectra reported in figure 2A. The noisy region between 1100 and 1200 cm^{-1} can be related to Si-O stretching modes associated to the presence of residual O atoms in the infrared window. Note also that there are no positive bands for adsorbed perchlorate anions around 1100 cm^{-1}, which can be clearly observed in the ATR-SEIRA spectra collected in CA-free perchloric acid solutions [65]. Instead, a negative band appears at this frequency value. This behavior suggests the presence of some amount of adsorbed perchlorate at the reference potential (0.30 V). This species would be displaced at more positive potentials due to the strong adsorption from species coming from CA, which hinders the co-adsorption of perchlorate anions for potentials above 0.30 V.

ATR-SEIRA spectra have also been collected at potentials between 0.30 V and 0.10 V, i.e. in the potential region where the redox peak pair was observed in Figure 1 (curve b1 in inset A). The spectra presented in figure 3A were obtained during a potential scan from 0.30V to 0.10 V and back to 0.30 V. They show a positive band at ca. 1610-1620 cm^{-1} (accompanied by the corresponding band at ca. 3480 cm^{-1}, not shown) reflecting the incorporation of weakly hydrogen-bonded water molecules as the electrode potential is decreased. Besides, a sharp band at ca. 1697 cm^{-1} and a feature at ca. 1257 cm^{-1} appear with intensities that also increase when decreasing the electrode potential. The intensities of all these bands decrease when the electrode potential is scanned up back to 0.30 V. Other noticeable features in the spectra shown in figure 3A are small negative signals at ca. 1450-1460 and 1100 cm^{-1}. These features indicate, respectively, the presence of small amounts of adsorbates coming from CA as well as some co-adsorbed perchlorate anions when collecting the reference spectrum at 0.30 V.

The existence of one these reduction processes could be at the origin of the behavior described in this work, which, do not seem to take place in the case of squaric acid as concluded from the absence of similar voltammetric and spectroscopic features in the considered potential region.

The absorption bands observed in the potential range between 0.30 and 0.10 V in Figure 3A suggest the formation of new adsorbed species upon reduction of CA or related species which is in connection with the voltammetric feature observed in Figure 1A. It is not clear at this stage whether this spectroelectrochemical response, which is not observed in the case of squaric acid,

is related to the reduction processes reported by Fleury et al [32]. In any case, the electrode reaction reported in Figures 1A and 3 seems to be reversible with respect to the electrode potential. Besides, the spectra collected between 0.30 and 0.80 V just after the potential excursion down to 0.10 V (Figure 3B) shows the same features for adsorbates coming from CA that those described above in the case of the experiments where the electrode potential is scanned directly from 0.30 to 0.80 V (see Figure 2A). The only difference between the spectra reported in figures 2A and 3B is related to the observation of a positive band for perchlorate anions that reaches a maximum for potentials around 0.50 V and disappears at more positive potentials. Note that the spectra in Figure 2A were collected after polarizing the electrode for a lapse of some tens of seconds at 0.30 V, needed for collecting the reference spectrum. This procedure could favor the adsorption of CA species with respect to the formation of adsorbed perchlorate. Under the conditions used in Figure 3B, perchlorate adsorption seems to be somewhat faster than that of CA in the potential region between 0.30 and 0.50 V.

The spectroelectrochemical behavior of CA at the gold thin film electrode in the potential range between 0.80 and 1.70 V has also been examined. The collected spectra during a slow positive-going scan in this potential region, which are reported in Figure 4, reflect that the main feature for species coming from CA still increases its intensity in the potential region between 0.80 and 1.00 V, in spite of the detection of oxidation currents in the CA-containing solution. Besides, the relative intensity of the band at ca. 1712 cm^{-1} increases in this potential region to the detriment of the feature at 1680 cm^{-1}. At potentials above 1.00 V, all these features vanish, being substituted by positive bands for the OH bending and stretching modes for strongly hydrogen-bonded interfacial water molecules at ca. 3456 and 1643 cm^{-1}[65]. The positive feature at ca. 3590 cm^{-1} lies in the same region characteristic of non-hydrogen-bonded OH group of the asymmetrically hydrogen-bonded water molecules in perchloric acid solutions [65]. Regarding other features that could be related to the eventually formed CA oxidation products, it has to be remarked the absence of the carbon dioxide in solution and adsorbed bicarbonate bands observed respectively at 2344 and 1415 cm^{-1} in the case of squaric acid oxidation at gold electrodes [43]. Instead, a broad absorption region can be observed between 1470 and 1280 cm^{-1} for potentials above 0.90 V that reaches maximum intensity at 1.10 V and disappears at higher potentials. At 1.10 V, two apparent maxima can be observed at 1363 and 1322 cm^{-1}. As mentioned above, it has been reported that the main oxidation product for croconic acid oxidation in aqueous media is leuconic acid [28, 34]. From the infrared spectra of this species [66, 67], namely from the absence of carbonyl bands, it was concluded that this species is fully hydrated in aqueous solutions[66], as a penta-(gem-diol). The frequencies of the extra features

observed in Figure 4 for the spectra collected around 1.10 V fit with some of the bands reported for (hydrated) leuconic acid [66, 67], thus suggesting that this species could be formed at the present experimental conditions.

5. DFT results and discussion

5.1. Optimized geometry of adsorbed croconate.

The most stable configurations of adsorbed discharged croconate species on Au(111) model surfaces that result from the geometry optimization procedure are shown in Figure 5 for coverages of 1/9, 2/9 and 1/3 croconate/gold surface atom. Table 1 summarizes some structural parameters for adsorbed croconate at the lower coverage studied. In this table, C1 and O1 refer to the carbon and oxygen atoms farthest from the gold surface whereas C4-5 and O4-5 stand for the atoms closest to the surface. Numbering of C and O atoms is given in Scheme 1. Table 2 summarizes the geometrical parameters for the optimized geometries of the croconate anion, the neutral cyclopentanpentone (sometimes referred as leuconic acid) and croconic acid, in the gas phase, for the sake of comparison.

The optimized structure of adsorbed croconate corresponds to a bidentate configuration, with bonding through two oxygen atoms placed near on-top positions irrespective of croconate coverages. As indicated above, it was checked for the lower coverage case that this result was also the same irrespective of the starting geometry before optimization. From the variety of values for the C-C and C-O bond lengths in Table 1 in comparison with values for croconate and cyclopentanpentone species in the gas phase (see Table 2), it is evident that the interaction of these two oxygen atoms with the gold atoms, leads to a rearrangement of the electronic density that causes a lowering of symmetry, from the D_{5h} point group of the free croconate anion (with two negative charges), to an adsorbate structure with C_{2v} symmetry. The latter is characterized by a C_2 symmetry axis (that coincides with the direction of the C-O bond normal to the metal surface), one vertical mirror plane σ_v that coincides with the molecular plane, and an additional vertical mirror plane $\sigma_{v'}$, that is mutually perpendicular to the previous one, and to the metal surface. No additional symmetry elements are found.

A first approach to the analysis of the calculated C-O and C-C bond lengths for adsorbed croconate can be done by comparing with tabulated typical bond lengths [68]. This comparison indicate that the 'upper' part of the adsorbate can be described as formed by three carbonyl groups connected by single C-C bonds (that have a typical C-C length value of 154 pm [68]). The

C-C bonds are shorter the closer they are to the metal (148 pm for the C2-C4 and C3-C5 bonds, and finally, 144 pm for the C4-C5 bond, that is parallel to the surface). These latter bond lengths are, however, significantly longer than the typical one for a double C=C bond (134 pm) [68]. Regarding the C-O distances for atoms 1-3, they agree well with those of carbonyl moieties (122 pm [68]) while those involving the oxygen atoms bonded to the metal are slightly longer (127 pm), but far from the range for single C-O bond (143 pm) [46]. This behavior is also very similar to that previously reported for adsorbed squarate [42, 43]. On the other hand, a comparison with the calculated values reported in table 2 for related species in the gas phase, shows that the changes in molecular structure caused by the adsorption of croconate lead to a symmetry and geometry that somewhat resemble those of croconic acid in the gas phase. In particular, most of the C-C and C-O bond lengths are very close to the counterparts in the gas-phase croconic acid. The resemblance is not so close for the bonds involving C4, C5, O4 and O5. In the adsorbed croconate, the bonding of the two oxygens to the metal causes a decrease in the bonding order of these C-O moieties (which appear slightly elongated with respect to the C-O bond length in gas phase croconate, but are shorter than the C-O bond in the enolic groups of croconic acid). The C4-C5 distance is slightly shorter for gas phase croconic acid, indicating a stronger bond than for the respective atoms in the adsorbed croconate.

The internal geometry (bond lengths and angles) of the carbonyl moieties in adsorbed croconate does not change significantly when going from coverage 1/9 to coverage 1/3. However, the oxygen-gold distances increase with coverage, from a value of around 227-229 pm at low coverage (θ = 1/9), increasing to 228-232 pm (θ = 2/9) and finally reaching 241-243 pm for the highest coverage studied in this paper (θ = 1/3). Note that the Au-O distances for adsorbed squarate at coverage 1/9 were 239-244 pm [42, 43]).

The increase in coverage also causes changes on the angle formed by the molecular plane with respect to the surface, and on its alignment with the dense surface metal rows (see Figure 5). In the case of the 1/9 coverage, the periodic boundary replicas are sufficiently far from each other as to not significantly influence the adsorption geometry. In that case, the molecular plane is perpendicular to that of the metal surface, and additionally, a good alignment with the surface dense metal rows is observed. When the coverage is increased to θ=2/9, the molecular planes of two neighboring croconate species are no longer parallel. Instead, they are tilted as a consequence of a significant increase in the separation of the part of the adsorbates that lie farthest from the surface. That distance amounts to 472 pm for the non-coordinated oxygen atoms, much longer than the separation between adjacent metal rows (where the oxygen atoms are bonded), 295 pm. This behavior is attributed to electrostatic repulsions between the pi-

electron densities of neighboring adsorbates. The increase of the Au-O distances when increasing CA coverage is also consistent with this interpretation that implies a decrease in the stabilization upon adsorption when high coverage is attained. The destabilization could also be partially caused by the changes in electronic structure of the bonding to the surface through the oxygen atoms.

If the coverage is further increased (up to 1/3), the molecular planes of the adsorbates are again perpendicular to the surface, with no tilting from the surface normal. This results from the symmetric compensation of the repulsions from both sides of each adsorbate. It is evident, however, that a misalignment of the molecular plane with respect to the metal dense rows exists. This 'twist' of the bonding direction is related to a slight displacement of the oxygen atoms from the perfect on-top positions towards the nearest fcc 3-fold hollow sites.

5.2. Harmonic vibrational frequencies for adsorbed croconate.

Table 3 summarizes the calculated harmonic vibrational frequencies (above 1200 cm^{-1}) of the croconate adsorbates at various coverage values, obtained for the optimized geometries shown in Figure 5. In the assignments, only the main contribution to each of the normal modes is given, as these involve complex combinations of atomic movements in the croconate adsorbate. A complete theoretical analysis of the vibrational normal modes of the CA adsorbate is beyond the scope of this paper. Moreover, the striking difference in symmetry means that the contributions to the normal modes are very different for the gas and adsorbed phase and the comparison of the corresponding vibrational features is far from being straightforward.

For the lower coverage (θ = 1/9) considered, the calculated infrared spectrum is relatively simple. In agreement with C-O distances discussed above, bands above 1650 cm^{-1} can be assigned to C=O stretching bands involving the C1-O1 (1754 cm^{-1}) and C2-O2 + C3-O3 (1723 and 1657 cm^{-1}) moieties. The vibrational mode at 1657 cm^{-1} would be infrared inactive since the corresponding variation of the dynamic dipole for this asymmetric mode would lie parallel to the metal surface, thus not fulfilling the surface selection rule both in IRRAS [69] and SEIRAS [70] experiments. Regarding the coordinated moiety of adsorbed croconate, the corresponding symmetric O4-C4-C5-O5 stretching would be infrared active (giving rise to an absorption band at 1498 cm^{-1}), whereas the corresponding asymmetric mode would be infrared inactive. Lower C-O stretching frequencies in comparison to the stretching bands above 1700 cm^{-1} correlate well with the calculated higher C-O bond lengths that are indicative of a decreased bond orders, that should in turn have lower values of force constants.

Additional complexity in the spectra of adsorbed croconate comes for higher coverage as a consequence of the relative phases of the vibrations of neighboring adsorbates for collective vibrational surface modes that causes band splitting and shifting as a consequence of the vibrational couplings. As a general trend, the couplings arising upon increasing coverage in dense adlayers cause the splitting of each of the frequencies for the low coverage, into a higher frequency due to the in-phase vibrations of neighboring adsorbed CA species, and a lower frequency coming from the coupling of the vibrations in an out-of-phase manner. Especially remarkable is the extent of the splitting and the strong shift calculated theoretically for a coverage of θ =1/3. In the case of the modes with main contributions due to the O4-C4-C5-O5 stretches, a stronger blue shift is obtained (around 120 cm^{-1}) for the asymmetric mode. This increase in frequency is in agreement with the elongation of the O-Au distances discussed above, that indicate a weaker adsorbate-surface bonding interaction. This is paralleled by changes in the O4-C4 distance (and its symmetry equivalent one, O5-C5), that are slightly shorter at higher coverage, indicating a stronger C-O bond (which results in a higher force constant and vibrational frequency).

5.3. Comparisons of theoretical frequencies for discharged adsorbed croconate and experimental spectra for thin films electrodes in CA-containing solutions.

As described above, the ATR-SEIRA spectra obtained for gold thin-film electrodes in CA-containing solutions between 0.30 and 0.80 V show a main band a 1470-1505 cm^{-1} accompanied by a couple of smaller features appearing in the range between 1680 and 1715 cm^{-1}. These spectral features can be compared in Figure 2B with spectra collected for SQA under similar experimental conditions, showing absorption bands at 1542 and 1774 cm^{-1} for low coverages (spectrum c) with an additional feature at ca. 1639 cm^{-1} for high coverages (spectrum b) [43]. According to DFT calculations for adsorbed squarate [42, 43], both the features at 1542 and 1639 cm^{-1} correspond to the C-O stretching of the metal-coordinated OCCO moiety which, for higher squarate coverage, undergoes splitting due to lateral dipole coupling, giving rise to in-phase and out-of-phase collective modes.

Comparison of the experimental values with the calculated frequencies for the lowest considered croconate coverage (Θ=1/9) show a relatively good agreement between the frequency value of the main experimental band and that calculated for the symmetric O4-C4-C5-O5 stretch. The observation of the two experimental features above 1650 cm^{-1} can be

connected to the two calculated frequency values for C1-O1 and O2-C2+C3-O3 stretching frequencies, respectively. The differences between the experimental and calculated frequencies are around 2-3 %, which is within the expected range for the error in the calculated values (see above). On the other hand, the aforementioned assignments for adsorbed croconate are consistent with those reported for adsorbed squarate at low coverage with the two features at ca. 1689 and 1712 cm^{-1} (instead of a single feature for adsorbed squarate) being related to the two kind of uncoordinated C-O moieties (instead of one in the case of squarate).

The inspection of the spectra reported in Figure 2A indicates that the main potential-dependent effect on the experimental spectra is the increase in the intensity of the observed features (plots of the corresponding integrated band intensities are given as supplementary material (Figure S1)). This can be understood as the result of an increase in the croconate coverage in the potential range between 0.30 and 0.80 V. This intensity increase is accompanied by a potential-dependent shift of the experimental frequencies, reported in Figure 2D. As in the case of squarate anions [42, 43], the frequency shift is higher for the lower frequency feature (with an average tuning rate around 95 $cm^{-1}\cdot V^{-1}$), which involves coordinated oxygen atoms. The intensity and band frequency increases of this band are paralleled by a noticeable broadening. Regarding the two carbonyl bands for adsorbed croconate, it has to be remarked that they undergo opposite frequency shifts as a function of the electrode potential (see Figure 2C). Tuning rates are around +20 and -30 $cm^{-1}\cdot V^{-1}$ for the features at around 1710 and 1680 cm^{-1} (see the corresponding plots in Figure 2D). Note also that the low-frequency carbonyl feature appears first for the less positive potential values but the relative intensity of the high-frequency increases as the electrode potential increases (see figure 2D and the plots in Figure S1).

As discussed for other adsorbed species [71], the existence of some Stark effect on the band frequencies could be considered to be at the origin of the reported frequency shifts. The theoretical prediction of this effect would require calculations with different values of applied electric field, and is not considered here. However, the observed frequency shifts can also be connected to the potential-dependent coverage changes. In this respect, the splitting of vibrational modes predicted by the DFT calculations for increasing CA coverages (see above) should be taken into account. The existence of in-phase and out-of-phase collective modes for the higher coverages (which are characterized by frequency values which are, respectively, higher and lower than those for lower coverage) are probably responsible for the observed broadening of the band in the range for O4-C4-C5-O5 symmetric stretch. Vibrational coupling effects could also contribute to the observed behavior for the features at around 1710 and 1680 cm^{-1} (related to the C1O1 and symmetric C2O2+C3O3 stretches, respectively). The relative

increase and upward shift of the former band would be related to an increasing contribution from in-phase modes as the electrode potential (and thus the croconate coverage) increases. On the contrary, an increasing contribution of out-of-phase modes for the band at ca. 1680 cm^{-1} could be at the origin of its downward frequency shift.

It has to be noted that the heterogeneity of the electrode surface and the eventual existence of patches with different local CA coverages makes difficult a complete description of the experimental results on the basis of the DFT calculations reported in this work. These calculations could be extended by considering this complexity as well as the eventual coadsorption of hydrogencroconate species, which is one of the predominant species present in the working solution.

6. Conclusions

A combined spectroelectrochemical and computational study of the adlayers formed on Au electrode surfaces in contact with acidic croconic acid-containing solutions has been carried out. In the potential region prior to the oxidation of the CA, croconate species has been spectroscopically detected on gold thin-layer electrodes. According to DFT calculations, a feature around 1470-1504 cm^{-1} in the ATR-SEIRA spectra, would correspond to the symmetric OCCO stretching modes involving the metal-coordinated oxygen atoms O4-C4+C5-O5 of croconate adsorbed in a bidentate configuration. Bands at ca 1712 cm^{-1} and 1689 cm^{-1}could be assigned to the stretch of the C1-O1 (that farthest from the electrode surface) and that arising the symmetric combination of the C2-O2 and C3-O3 stretches, respectively. DFT calculations show the existence of some tilting of the molecular plane at intermediate coverages which are related to electrostatic repulsions between the pi-electron densities of neighboring adsorbates. Even if we can neither completely rule out the presence of adsorbed hydrogencroconate anions or CA molecules at the electrode surface, we can conclude from the present results that adsorbed croconate seems to be the prevailing adsorbate coming from CA. DFT calculations for croconate adlayers at various coverage values suggest that the observed broadening and shifting of the adsorbate bands for increasing electrode potentials are related to collective modes with different degrees of shifting and dephasing, arising from the dipole coupling for neighbor adsorbed croconate. The different sign of the frequency tuning rates with electrode potentials for the two carbonyl bands is in agreement with the trends predicted by their calculated harmonic frequencies at different coverage values. More work is in progress, including ATR-SEIRAS experiments in deuterium oxide solutions with various CA concentrations, as well as

additional DFT calculations, in order to test the possible presence of other adsorbed species coming from croconic acid (such as hydrogencroconate, for instance), at gold electrodes.

Another point explored in this paper was the spectroelectrochemical behavior of the gold electrodes in the croconic acid oxidation region. At the onset of CA oxidation (around 0.85 V), the ATR-SEIRA spectra show a further increase in the croconate coverage which falls to nearly cero for potentials around 1.10 V. In this potential region, new features can be detected, which could be associated to the formation of some reaction intermediates. In order to assess whether these species are related to leuconic acid (the proposed CA oxidation product), further DFT calculations would be needed. In any case it seems that the complete oxidation of CA to carbon dioxide, which can be detected more easily in external reflection experiments with a thin layer configuration, is less favored than in the case of squaric acid (SQA) for which adsorbed bicarbonate (formed from dissolved carbon dioxide coming from CA oxidation) was detected from the ATR-SEIRA spectra.

Finally, the voltammetric and ATR-SEIRAS results reported in this work have shown the existence of a redox surface process, not previously observed in the case of squaric acid, which involves the formation of a reduced adsorbate. The nature of this species will be the subject of a future work involving additional DFT calculations of the optimized geometries and the corresponding vibrational frequencies for a variety of possible reduced CA species.

Acknowledgements

The authors are indebted to Mr. Jorge Martínez-Olivares, who carried out preliminary research work in our group on the electrochemical behavior of CA at gold electrodes. The funding by Ministerio de Ciencia e Innovación through project PID2019-105653GB-100, by Conselleria d'Innovació, Universitats, Ciència i Societat Digital (Generalitat Valenciana, project PROMETEO/2020/063) and by the University of Alicante (VIGROB-263) is acknowledged.

Figure captions

Figure 1. (a) Cyclic voltammograms obtained in 0.1 M $HClO_4$ solutions for a gold thin film electrode deposited on the silicon windows used for the ATR-SEIRAS experiments. Curves (b) in the main panel and in inset (A) were recorded in solutions containing 10 mM croconic acid (CA) whereas that shown in the inset (B) was obtained in a 10 mM squaric acid (SQA) solution. Sweep rate: 50 $mV \cdot s^{-1}$.

Figure 2. (A) Potential-difference ATR-SEIRA spectra collected with a gold thin film electrode in a 10mMCA + 0. 1 M $HClO_4$ solution. The electrode potential was swept at 2 $mV \cdot s^{-1}$ from 0.30 to 0.80 V. Each spectrum corresponds to a 20 mV interval around the indicated values (see the experimental section for details). (B) Comparison of the ATR-SEIRA spectra collected for the CA- (a) and SQA-containing (b,c) solutions (10 mM in 0.1 M $HClO_4$). Sample potentials were 0.80 V (a,b) and 0,50 V (c) (C) Enlargement between 1650 and 1750 cm^{-1} of the spectra plotted in (A). The potential-dependent frequency values shown in (D) for the main bands for CA were measured from spectra collected under static conditions at the corresponding potentials. The reference spectra were collected at 0.30 V in the CA-containing solution and at 0.10 V in the SQA-containing solution.

Figure 3. (A) Potential-difference ATR-SEIRA spectra collected with a gold thin film electrode in a 10mMCA + 0. 1 M $HClO_4$ solution during a potential sweep from 0.30 to 0.10 V and back to 0.30V (bottom to top). (B) Potential-difference ATR-SEIRA spectra collected in the same solution during the subsequent sweep from 0.30 to 0.80 V. Each spectrum corresponds to a 20 mV interval around the indicated values (see the experimental section for details).The reference spectra were collected at 0.30 V in the CA-containing solution just before starting the potential sweep down to 0.10 V.

Figure 4. Potential-difference ATR-SEIRA spectra collected at potentials above 0.80 V with a gold thin film electrode in a 10 mM CA + 0. 1 M $HClO_4$ solution during a potential sweep from 0.30 to 1.70 V. Each spectrum corresponds to a 20 mV interval around the indicated values (see the experimental section for details). The reference spectrum was collected at 0.30 V in the CA-containing solution.

Figure 5. Lateral and top views of the optimized geometries of adsorbed croconate on Au(111) surfaces, at different coverages: A) $\theta = 1/9$; B) $\theta = 2/9$; C) $\theta = 1/3$.

Scheme 1. Molecular structure and notation for adsorbed croconate on Au(111) surface.

Reference list.

[1] R. West, J. Niu, Oxocarbons and their reactions, in: J. Zabicky (Ed.) The Chemistry of the Carbonyl Group, John Wiley & Sons, 1970, pp. 241-275.

[2] R. West, Ed., Oxocarbons, Academic Press, New York, 1980.

[3] G. Seitz, P. Imming, Oxocarbons and pseudooxocarbons, Chem. Rev., 92 (1992) 1227-1260.

[4] L.M. Schwartz, R.I. Gelb, J.O. Yardley, Aqueous dissociation of croconic acid, J. Phys. Chem., 79 (1975) 2246-2251.

[5] Z.X. Wong, H.H. Abdallah, Gas-phase acidity and liquid phase pKa calculations of some cyclic oxocarbon acids (CnOnH2 (n = 3, 4, 5, 6)): a theoretical investigation, Acta Chim. Slov., 59 (2012) 273-280.

[6] S. Mukhopadhyay, M. Gutmann, F. Fernandez-Alonso, Hydrogen-bond structure and anharmonicity in croconic acid, Phys. Chem. Chem. Phys., 16 (2014) 26234-26239.

[7] J. Hooper, D.A. Kunkel, E. Zurek, A. Enders, Interplay between Hydrogen Bonding, Epitaxy, and Charge Transfer in the Self-Assembly of Croconic Acid on Au(111) and Ag(111), J. Phys. Chem. C, 119 (2015) 26429-26437.

[8] D.A. Kunkel, J. Hooper, B. Bradley, L. Schlueter, T. Rasmussen, P. Costa, S. Beniwal, S. Ducharme, E. Zurek, A. Enders, 2D Cocrystallization from H-Bonded Organic Ferroelectrics, J. Phys. Chem. Lett., 7 (2016) 435-440.

[9] D.P. Miller, P.S. Costa, J.D. Teeter, A. Sinitskii, A. Enders, J.G.M. Hooper, Seeking Out Heterogeneous Hydrogen Bonding in a Self-Assembled 2D Cocrystal of Croconic Acid and Benzimidazole on Au(111), J. Phys. Chem. C, 125 (2021) 2403-2410.

[10] D. Braga, L. Maini, F. Grepioni, Croconic acid and alkali metal croconate salts: some new insights into an old story, Chem. - Eur. J., 8 (2002) 1804-1812.

[11] J.D. Dunitz, A. Gavezzotti, S. Rizzato, "Coulombic Compression", a Pervasive Force in Ionic Solids. A Study of Anion Stacking in Croconate Salts, Cryst. Growth Des., 14 (2014) 357-366.

[12] S. Horiuchi, Y. Tokunaga, G. Giovannetti, S. Picozzi, H. Itoh, R. Shimano, R. Kumai, Y. Tokura, Above-room-temperature ferroelectricity in a single-component molecular crystal, Nature (London, U. K.), 463 (2010) 789-792.

[13] D. Di Sante, A. Stroppa, S. Picozzi, Structural, electronic and ferroelectric properties of croconic acid crystal: a DFT study, Phys. Chem. Chem. Phys., 14 (2012) 14673-14681.

[14] S. Mohapatra, V. Da Costa, G. Avedissian, J. Arabski, W. Weber, M. Bowen, S. Boukari, Robust ferroelectric properties of organic croconic acid films grown on spintronically relevant substrates, Mater. Adv., 1 (2020) 415-420.

[15] X. Jiang, H. Lu, Y. Yin, X. Zhang, X. Wang, L. Yu, Z. Ahmadi, P.S. Costa, A.D. DiChiara, X. Cheng, A. Gruverman, A. Enders, X. Xu, Room temperature ferroelectricity in continuous croconic acid thin films, Appl. Phys. Lett., 109 (2016) 1029021-1029024.

[16] F. Colmenero, Anomalous mechanical behavior of the deltic, squaric and croconic cyclic oxocarbon acids, Mater. Res. Express, 6 (2019) 0456101-04561034.

[17] F. Colmenero, Addendum: anomalous mechanical behavior of the deltic, squaric and croconic cyclic oxocarbon acids, Mater. Res. Express, 6 (2019) 694011-694013.

[18] F. Colmenero, R. Escribano, Thermodynamic, Raman Spectroscopic, and UV-Visible Optical Characterization of the Deltic, Squaric, and Croconic Cyclic Oxocarbon Acids, J. Phys. Chem. A, 123 (2019) 4241-4261.

[19] E.A. Milan-Garces, S.L. Georgopoulos, A.C. Sant'Ana, G.F.S. Andrade, L.F.C. de Oliveira, Chemical behavior of croconic acid coordinated to Co(II) adsorbed on silver surface, J. Raman Spectrosc., 49 (2018) 1174-1183.

[20] G.M.A. Junqueira, W.R. Rocha, W.B. De Almeida, H.F. Dos Santos, Theoretical analysis of the oxocarbons: structure and spectroscopic properties of croconate ion and its coordination compound with lithium, Phys. Chem. Chem. Phys., 3 (2001) 3499-3505.

[21] C. Luo, R. Huang, R. Kevorkyants, M. Pavanello, H. He, C. Wang, Self-Assembled Organic Nanowires for High Power Density Lithium Ion Batteries, Nano Lett., 14 (2014) 1596-1602.

[22] T. Kikuchi, D. Nakajima, J. Kawashima, S. Natsui, R.O. Suzuki, Fabrication of anodic porous alumina via anodizing in cyclic oxocarbon acids, Appl. Surf. Sci., 313 (2014) 276-285.

[23] N.E. Larm, J.B. Essner, K. Pokpas, J.A. Canon, N. Jahed, E.I. Iwuoha, G.A. Baker, Room Temperature Turkevich Method: Formation of Gold Nanoparticles at the Speed of Mixing Using Cyclic Oxocarbon Reducing Agents, J. Phys. Chem. C, 122 (2018) 5105-5118.

[24] I.V. Kurdiukova, A.V. Kulinich, A.A. Ishchenko, Near-infrared squarate and croconate dianions derived from tetranitrofluorene, New J. Chem., 36 (2012) 1564-1567.

[25] R.R. Avirah, K. Jyothish, D. Ramaiah, Infrared absorbing croconaine dyes: Synthesis and metal ion binding properties, J. Org. Chem., 73 (2008) 274-279.

[26] L.M. Doane, A.J. Fatiadi, Electrochemical oxidation of croconate salts: evidence of the chemical equivalence of the carbonyl oxygen atom and the dicyanomethylene group, Angew Chem Int Ed Engl, 21 (1982) 2.

[27] L.M. Doane, A.J. Fatiadi, Electrochemical oxidation of several oxocarbon salts in N,N-dimethylformamide, J. Electroanal. Chem., 135 (1982) 193-209.

[28] P.-L. Fabre, P. Castan, D. Deguenon, N. Paillous, A photo-oxidation of croconic acid into oxalic acid, Can. J. Chem., 73 (1995) 1298-1304.

[29] P.-L. Fabre, F. Dumestre, B. Soula, A.-M. Galibert, Spectroelectrochemical behavior in dimethylformamide of pseudo-oxocarbons dianions derived from the croconate dianion, Electrochim. Acta, 45 (2000) 2697-2705.

[30] Z.-M. Xue, C.-H. Chen, Theoretical study of electrical and electrochemical properties of cyclopentanepentaone and its dicyanomethylene derivatives, Int. J. Quantum Chem., 107 (2006) 637-646.

[31] M. Fleury, The reduction products of croconic acid, Compt. Rend., 258 (1964) 1512-1515.

[32] M.B. Fleury, P. Souchay, M. Gouzerh, P. Gracian, Reduction of croconic acid at the mercury electrode; reaction mechanism and characterization of the reduction products, Bull. Soc. Chim. Fr., (1968) 2562-2572.

[33] F. Gracian, M.B. Fleury, P. Souchay, Croconic acid derivatives. II. Pinacolic-derivatives formed by reduction of croconic acid (R) : RH--RH, RH--RH3, and RH3--RH3, Bull. Soc. Chim. Fr., (1969) 4590-4595.

[34] D. Sazou, G. Kokkinidis, Electrochemical oxidation of squaric and croconic acids on platinum and platinum surfaces modified by underpotential heavy metal monolayers in acid solutions, Can. J. Chem. , 65 (1987) 397-403.

[35] R. Albalat, J. Claret, J.M. Orts, J.M. Feliu, Electrochemical behavior of squaric acid on single-crystal platinum electrodes with basal orientations in aqueous sulfuric acid medium, J. Electroanal. Chem., 334 (1992) 291-307.

[36] A. Rodes, J.M. Pérez, J.M. Orts, J.M. Feliu, A. Aldaz, FTIR study of the electrochemical behavior of squaric acid on polycrystalline platinum electrodes in 0.5M sulfuric acid, J. Electroanal. Chem., 352 (1993) 345-352.

[37] J.M. Orts, A. Rodes, R. Carbó, R. Albalat, J. Claret, Electrochemical behavior of oxocarbons on single crystal platinum electrodes Part II . Croconic acid oxidation on Pt(S)-[n(100)x(111)] surfaces in 0.5 M sulfuric acid medium, J. Electroanal. Chem., 376 (1994) 101-108.

[38] R. Carbo, R. Albalat, J. Claret, J.M. Orts, A. Rodes, J.M. Perez, Electrochemical behavior of oxocarbons on single crystal platinum electrodes. Part 3. Croconic acid oxidation on Pt(111) surfaces in acid medium, J. Electroanal. Chem., 404 (1996) 161-169.

[39] R. Carbó, R. Albalat, J. Claret, J.M. Orts, A. Rodes, Electrochemical behaviour of oxocarbons on single crystal platinum ele ctrodes .4. Rhodizonic acid in 0.5 M sulphuric acid medium, J. Electroanal. Chem., 424 (1997) 185-196.

[40] A. Rodes, J.M. Orts, J.M. Pérez, J.M. Feliu, A. Aldaz, On the electrochemical behavior of squaric acid on Pt(hkl) electrodes in acid solutions: a voltammetric and in situ FTIRS study, J. Electroanal. Chem., 421 (1997) 195-204.

[41] R. Carbó, R. Albalat, J. Claret, Electrochemical behaviour of oxocarbons on single crystal platinum ele ctrodes - Part V. Tetrahydroxy-p-benzoquinone in 0.5 M sulphuric acid medium, J. Electroanal. Chem., 440 (1997) 57-64.

[42] W. Cheuquepán, J. Martinez-Olivares, A. Rodes, J.M. Orts, Squaric acid adsorption and oxidation at gold and platinum electrodes, J. Electroanal. Chem., 819 (2017) 178-186.

[43] W. Cheuquepán, A. Rodes, J.M. Orts, J.M. Feliu, Spectroelectrochemical and Density Functional Theory Study of Squaric Acid Adsorption and Oxidation at Gold Thin Film and Single Crystal Electrodes, J. Phys. Chem. C, 122 (2018) 22352-22365.

[44] L.M. Doane, A.J. Fatiadi, Electrochemical oxidation of croconic acid salts; proofs for the chemical equivalence of the carbonyl oxygen atom and the dicyanomethylene group, Angew. Chem., 94 (1982) 649-650.

[45] K. Ataka, M. Osawa, In situ infrared study of water-sulfate coadsorption on gold(111) in sulfuric acid solutions, Langmuir, 14 (1998) 951-959.

[46] T. Wandlowski, K. Ataka, S. Pronkin, D. Diesing, Surface enhanced infrared spectroscopy-Au(111-20 nm)/sulphuric acid - new aspects and challenges, Electrochim. Acta, 49 (2004) 1233-1247.

[47] J.M. Delgado, J.M. Orts, J.M. Pérez, A. Rodes, Sputtered thin-film gold electrodes for in situ ATR-SEIRAS and SERS studies, J. Electroanal. Chem., 617 (2008) 130-140.

[48] K.M. Neyman, F. Illas, Theoretical aspects of heterogeneous catalysis: Applications of density functional methods, Catal.Today, 105 (2005) 2-16.

[49] W. Cheuquepán, A. Rodes, J.M. Orts, J.M. Feliu, Spectroelectrochemical detection of specifically adsorbed cyanurate anions at gold electrodes with (111) orientation in contact with cyanate and cyanuric acid neutral solutions, J. Electroanal. Chem., 800 (2017) 167-175.

[50] W. Cheuquepan, A. Rodes, J.M. Orts, Cyanate and Cyanurate Adsorption at Silver Electrodes in Neutral Solutions: In Situ ATR-SEIRAS and DFT Studies, J. Phys. Chem. C, 124 (2020) 709-721.

[51] A. Rodes, J.M. Pérez, A. Aldaz, Vibrational Spectroscopy, in: W. Vielstich, H.A. Gasteiger, A. Lamm (Eds.) Handbook of Fuel Cells. Fundamentals, Technology and Applications., John Wiley & Sons Ltd., Chichester, 2003, pp. 191-219.

[52] J.M. Delgado, J.M. Orts, A. Rodes, ATR-SEIRAS study of the adsorption of acetate anions at chemically deposited silver thin film electrodes, Langmuir, 21 (2005) 8809-8816.

[53] J.P. Perdew, K. Burke, M. Ernzerhof, Generalized gradient approximation made simple, Phys.Rev.Lett., 77 (1996) 3865-3868.

[54] J.P. Perdew, K. Burke, M. Ernzerhof, Generalized gradient approximation made simple. [Erratum to document cited in CA126:51093], Phys.Rev.Lett., 78 (1997) 1396.

[55] G. Kresse, J. Hafner, Ab initio molecular dynamics of liquid metals, Phys.Rev.B, 47 (1993) 558-561.

[56] G. Kresse, J. Hafner, Ab initio molecular-dynamics simulation of the liquid-metal-amorphous-semiconductor transition in germanium, Phys.Rev.B, 49 (1994) 14251-14269.

[57] A. Eichler, J. Hafner, G. Kresse, J. Furthmuller, Relaxation and electronic surface states of rhodium surfaces, Surf. Sci., 352 (1996) 689-692.

[58] G. Kresse, J. Furthmuller, Efficiency of ab-initio total energy calculations for metals and semiconductors using a plane-wave basis set, Comput.Mater.Sci., 6 (1996) 15-50.

[59] P.E. Bloechl, Projector Augmented-Wave method, Phys.Rev.B, 50 (1994) 17953-17979.

[60] M. Methfessel, A.T. Paxton, High-precision sampling for Brillouin-zone integration in metals, Phys.Rev.B: Condens.Matter, 40 (1989) 3616-3621.

[61] H.J. Monkhorst, J.D. Pack, Special points for Brillouin-zone integrations, Phys. Rev. B, 13 (1976) 5188-5192.

[62] Jmol: an open-source Java viewer for chemical structures in 3D, in, http://www. jmol. org, 2015.

[63] M. Osawa, Dynamic processes in electrochemical reactions studied by Surface-Enhanced InfraRed Absorption Spectroscopy (SEIRAS), Bull.Chem.Soc.Jpn., 70 (1997) 2861-2880.

[64] R.F. Aroca, D.J. Ross, C. Domingo, Surface-Enhanced Infrared Spectroscopy, Appl. Spectrosc., 58 (2004) 324A-338A.

[65] K. Ataka, T. Yotsuyanagi, M. Osawa, Potential-dependent reorientation of water molecules at an electrode/electrolyte interface studied by Surface-Enhanced Infrared Absorption Spectroscopy, J. Phys. Chem., 100 (1996) 10664-10672.

[66] W.B. Person, D.G. Williams, Infrared spectra and the structures of leuconic acid and triquinoyl, J. Phys. Chem., 61 (1957) 1017-1018.

[67] A.J. Fatiadi, H.S. Isbell, W.F. Sager, Cyclic polyhydroxyketones I. Oxidation products of hexahydroxybenzene (benzenehexol), J. Res. Natl. Bur. Stand., Sect. A, 67A (1963) 153-162.

[68] D.R. Lide, Ed, CRC Handbook of Chemistry and Physics, 89th Edition, CRC Press, Boca Raton, FL, 2008.

[69] R.G. Greenler, Infrared study of adsorbed molecules on metal surfaces by reflection techniques, Journal of Chemical Physics, 44 (1966) 310-315.

[70] M. Osawa, K. Ataka, K. Yoshii, Y. Nishikawa, Surface-enhanced Infrared Spectroscopy : the origin of the absorption enhancement and band selection rule in the infrared spectra of molecules adsorbed on fine metal particles, Appl. Spectrosc., 47 (1993) 1497-1502.

[71] F.C. Nart, T. Iwasita, Static field effect on the band intensity of adsorbed sulfate ions, Electrochim. Acta, 41 (1996) 631-636.